

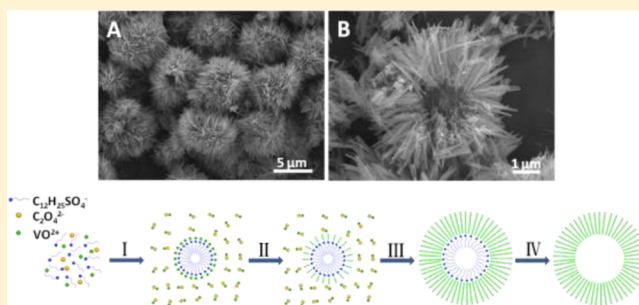
# VO<sub>2</sub> Nanowires Assembled into Hollow Microspheres for High-Rate and Long-Life Lithium Batteries

Chaojiang Niu,<sup>†</sup> Jiashen Meng,<sup>†</sup> Chunhua Han,<sup>\*</sup> Kangning Zhao, Mengyu Yan, and Liqiang Mai<sup>\*</sup>

State Key Laboratory of Advanced Technology for Materials Synthesis and Processing, WUT-Harvard Joint Nano Key Laboratory, Wuhan University of Technology, Wuhan 430070, China

**S** Supporting Information

**ABSTRACT:** Development of three-dimensional nanostructures with high surface area and excellent structural stability is an important approach for realizing high-rate and long-life battery electrodes. Here, we report VO<sub>2</sub> hollow microspheres showing empty spherical core with radially protruding nanowires, synthesized through a facile and controllable ion-modulating approach. In addition, by controlling the self-assembly of negatively charged C<sub>12</sub>H<sub>25</sub>SO<sub>4</sub><sup>-</sup> spherical micelles and positively charged VO<sup>2+</sup> ions, six-armed microspindles and random nanowires are also prepared. Compared with them, VO<sub>2</sub> hollow microspheres show better electrochemical performance. At high current density of 2 A/g, VO<sub>2</sub> hollow microspheres exhibit 3 times higher capacity than that of random nanowires, and 80% of the original capacity is retained after 1000 cycles. The superior performance of VO<sub>2</sub> hollow microspheres is because they exhibit high surface area about twice higher than that of random nanowires and also provide an efficient self-expansion and self-shrinkage buffering during lithiation/delithiation, which effectively inhibits the self-aggregation of nanowires. This research indicates that VO<sub>2</sub> hollow microspheres have great potential for high-rate and long-life lithium batteries.



**KEYWORDS:** Nanowires, hollow microspheres, ion-modulating, vanadium oxide, buffering, lithium batteries

Nanostructures have been widely studied and applied in the field of energy storage due to their instinct characteristic of nanoscale size increasing the surface area and reducing the diffusion length.<sup>1–5</sup> Low-dimensional nanostructures, including nanoparticles, nanowires, and nanosheets, have shown a large superiority in lithium batteries.<sup>6–12</sup> However, self-aggregation and pulverization of the low-dimensional nanostructures are still critical issues. In order to realize high surface area and excellent structural stability, various three-dimensional (3D) nanostructures have been further investigated for high-rate and long-life lithium batteries.<sup>13–21</sup> Nevertheless, it still remains a challenge to realize controllable synthesis of 3D nanostructures, which also seriously limits its further popularization.<sup>22–26</sup>

Vanadium oxides have been widely investigated as cathode materials for high-rate and long-life lithium batteries due to their high capacity and low cost.<sup>27–30</sup> In particular, B phase vanadium dioxide, denoted as VO<sub>2</sub> (B), attracts more interest because of its rapid lithium ion intercalation–deintercalation in double layers of V<sub>4</sub>O<sub>10</sub> structure for both organic and aqueous lithium batteries.<sup>31–36</sup> However, the fast capacity fading and the self-aggregation of VO<sub>2</sub> nanowires greatly preclude its large-scale applications.<sup>37–40</sup>

Here, we report a facile ion-modulating approach for synthesizing novel hollow microspheres which have empty spherical core with radially protruding VO<sub>2</sub> nanowires (Figure 1A). In such unique architecture, (1) nanowires can

theoretically expand and shrink freely on both radial and axial directions, and (2) the hollow microspheres can provide a buffering for self-expansion and self-shrinkage to effectively accommodate the volume variation during lithium intercalation–deintercalation, thus inhibiting the self-aggregation of nanowires, increasing the surface area, and improving the electrochemical performance. In addition, by controlling the charge balance of negatively charged C<sub>12</sub>H<sub>25</sub>SO<sub>4</sub><sup>-</sup> spherical micelles and positively charged VO<sup>2+</sup> ions, VO<sub>2</sub> six-armed microspindles and random nanowires are also synthesized as control experiments (Figure 1B and Figure S1).

Ion-modulating is conducted and achieved by changing the molar ratio of V<sub>2</sub>O<sub>5</sub> and H<sub>2</sub>C<sub>2</sub>O<sub>4</sub>.<sup>41</sup> When the molar ratio of V<sub>2</sub>O<sub>5</sub> and H<sub>2</sub>C<sub>2</sub>O<sub>4</sub> is 1:2.4, VO<sub>2</sub> nanowires self-assemble together, forming empty spherical core with radially protruding nanowires (Figure 2A,B). Such hollow microspheres are very uniform and a part of them are ringent, confirming the centers are hollow. The diameter of the inner pore is ~1 μm; the nanowires are uniform with a diameter of ~50 nm and length of ~2 μm. When the reacting ratio of V<sub>2</sub>O<sub>5</sub> and H<sub>2</sub>C<sub>2</sub>O<sub>4</sub> is decreased to 1:3, the resulting sample is six-armed microspindle, three nanosheets intersect with each other, and the intersection angle is ~60°. The nanosheets are homogeneous

**Received:** March 11, 2014

**Revised:** April 10, 2014

**Published:** April 17, 2014

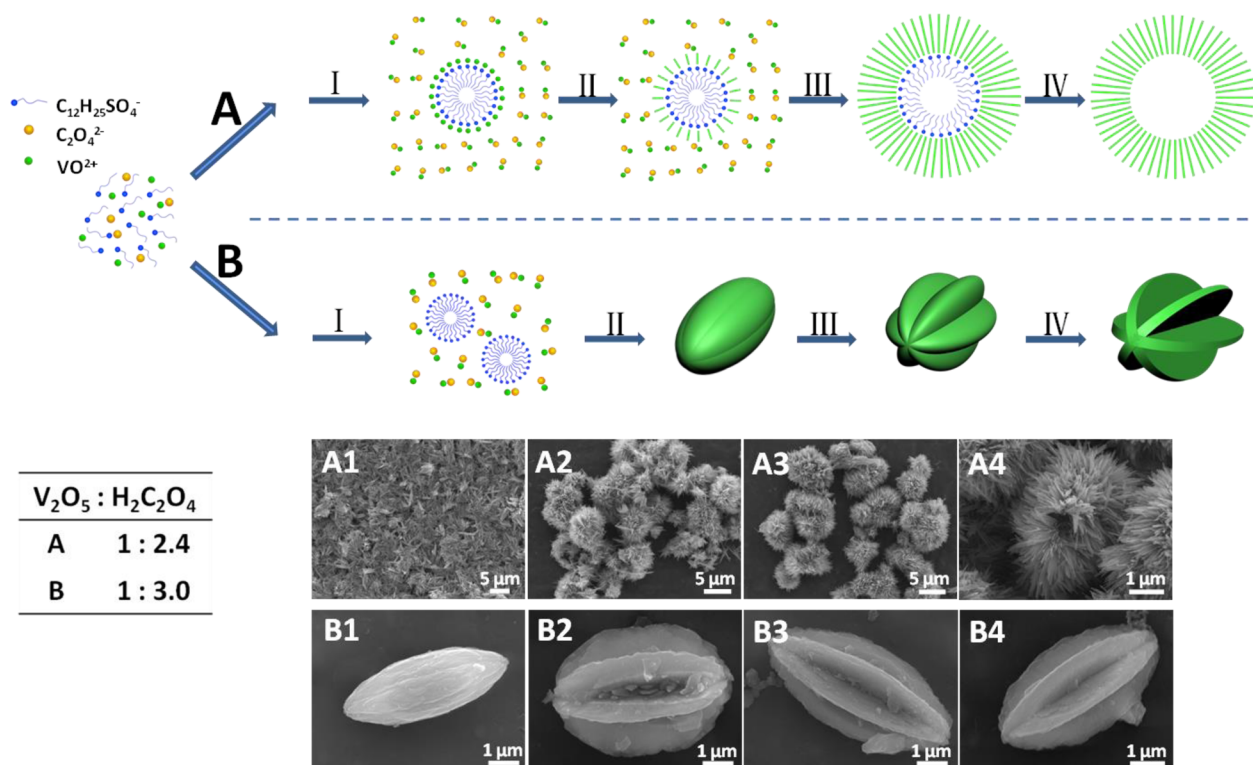


**Figure 1.** Schematic illustrations of formation process of hollow microspheres and six-armed microspindles via the ion-modulating method. (A1–A4) SEM images of hollow microspheres prepared at 6, 12, 18, and 24 h, respectively. (B1–B4) SEM images of six-armed microspindles prepared at 6, 12, 18, and 24 h, respectively.

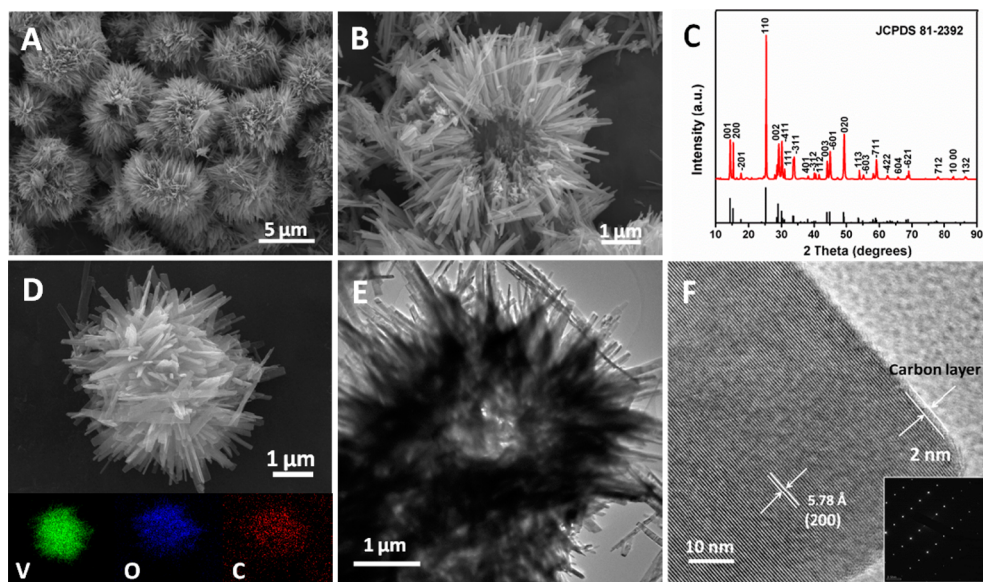


**Figure 2.** (A) SEM image of hollow microspheres assembled with nanowires. (B) SEM image of one ringent hollow microsphere having empty spherical core with radially protruding nanowires. (C) XRD pattern of hollow microspheres. (D) SEM image and EDS elemental mappings of hollow microspheres (vanadium, oxygen, and carbon elements are characterized). (E) TEM image of hollow microspheres. (F) HRTEM image of nanowire in hollow microspheres; inset of (F) is the corresponding SAED pattern.

with  $\sim 50$ – $100$  nm thickness and  $\sim 4$   $\mu\text{m}$  length (Figure S2A,B). After the ratio of  $V_2O_5$  and  $H_2C_2O_4$  is increased to 1:1.8,  $VO_2$  nanowires are dispersed randomly, with  $\sim 50$  nm diameter and  $\sim 2$   $\mu\text{m}$  length (Figure S2D,E).

The crystal structures of three representative samples were determined by X-ray diffraction (XRD) (Figure 2C and Figure S3). The patterns are identified as pure monoclinic  $VO_2$  (B)

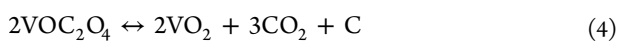
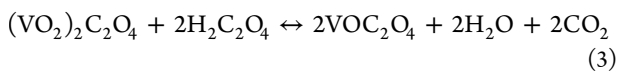
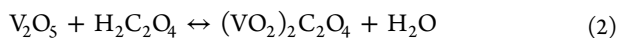
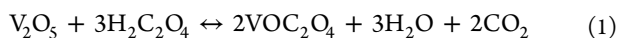
with the lattice parameters of  $a = 12.09$   $\text{\AA}$ ,  $b = 3.70$   $\text{\AA}$ ,  $c = 6.43$   $\text{\AA}$ ,  $\beta = 107.0^\circ$ ,  $C2/m$  space group. As shown in transmission electron microscopy (TEM) image (Figure 2E),  $VO_2$  hollow microspheres exhibit an empty spherical core with radially protruding nanowires. The high-resolution TEM (HRTEM) image shows clear lattice fringes with spacing of  $5.78$   $\text{\AA}$ , corresponding to the (200) lattice plane of  $VO_2$  (B) (Figure

Table 1. Different Dominant Reactions and Ions in the Precursor Solution

	V <sub>2</sub> O <sub>5</sub> :H <sub>2</sub> C <sub>2</sub> O <sub>4</sub>	dominant reaction	dominant positive ions	dominant negative ions	valence state of vanadium	color of the precursor	structure
A	1:2.4	reduction	VO <sup>2+</sup>	C <sub>12</sub> H <sub>25</sub> SO <sub>4</sub> <sup>-</sup>	+4	light blue	hollow microspheres
B	1:3.0	reduction	VO <sup>2+</sup>	C <sub>2</sub> O <sub>4</sub> <sup>2-</sup>	+4	blue	six-armed microspindles
C	1:1.8	neutralization	Na <sup>+</sup>	C <sub>12</sub> H <sub>25</sub> SO <sub>4</sub> <sup>-</sup>	+5	light green	random nanowires

2F). The single crystalline nature of single nanowire in hollow microspheres is also confirmed by selected-area electron diffraction (SAED) measurement. Furthermore, a uniform thin carbon layer of ~2 nm covers the surface of the VO<sub>2</sub> nanowires, which is proved by HRTEM image, energy dispersive X-ray spectra (EDS) elemental mappings (Figure 2D), and thermogravimetric/differential scanning calorimeter (TG-DSC) (Figure S4). The mass percentage of carbon in hollow microspheres is ~6.26% measured by TG-DSC, consistent with the result of 6.74% calculated from the reaction equation.

In order to understand the formation processes of these three nanostructures, a series of control experiments were designed and carried out. The morphologies of samples obtained in different reacting conditions were characterized by field-emission scanning electron microscope (FESEM). When the molar ratio of V<sub>2</sub>O<sub>5</sub> and H<sub>2</sub>C<sub>2</sub>O<sub>4</sub> is 1:2.4, different morphologies are obtained with the reacting time increasing from 6 to 12, 18, and 24 h (Figure 1A). When the reacting time is 6 h, most of VO<sub>2</sub> nanowires are dispersed and tend to assemble together (Figure 1A1). Then with the reacting time increases to 12 h, a lot of microspheres are obtained (Figure 1A2). After 18 h, the microspheres become uniform (Figure 1A3). At last, hollow uniform microspheres are formed at 24 h (Figure 1A4). At the same time, in order to understand the specific role of surfactant C<sub>12</sub>H<sub>25</sub>SO<sub>4</sub>Na, the amount of C<sub>12</sub>H<sub>25</sub>SO<sub>4</sub>Na were also modulated from 0 to 0.5, 1.7, and 3.5 mmol (Figure S5). It obviously demonstrates that the nanowires do not surround together forming microspheres but separate from each other without C<sub>12</sub>H<sub>25</sub>SO<sub>4</sub>Na (Figure S5A). After C<sub>12</sub>H<sub>25</sub>SO<sub>4</sub>Na (0.5 mmol) is added, a small part of microspheres are formed and assembled with nanowires, while most of the nanowires are still at random (Figure S5B), proving C<sub>12</sub>H<sub>25</sub>SO<sub>4</sub>Na is insufficient. When the amount of C<sub>12</sub>H<sub>25</sub>SO<sub>4</sub>Na reaches 1.7 mmol, all nanowires form uniform hollow microspheres (Figure S5C). By continuing to increase the amount of C<sub>12</sub>H<sub>25</sub>SO<sub>4</sub>Na to 3.5 mmol, the microspheres are inhomogeneous (Figure S5D), proving C<sub>12</sub>H<sub>25</sub>SO<sub>4</sub>Na is superfluous. To sum up, uniform hollow microspheres are obtained at the condition of 1.7 mmol of C<sub>12</sub>H<sub>25</sub>SO<sub>4</sub>Na and 24 h of reacting time.



Combined with the liquid-crystal templating (LCT) mechanism and cooperative formation mechanism (CFM),<sup>42,43</sup> the formation process can be illustrated as follows (Figure 1A). According to the eqs 1–4,<sup>32,39</sup> VO<sup>2+</sup> ions are surplus when the molar ratio of V<sub>2</sub>O<sub>5</sub> and H<sub>2</sub>C<sub>2</sub>O<sub>4</sub> is 1:2.4, which is also proved by the light blue color of the precursor

(Figure S6). Two-thirds of the H<sub>2</sub>C<sub>2</sub>O<sub>4</sub> decompose into CO<sub>2</sub> and H<sub>2</sub>O, so the number of C<sub>2</sub>O<sub>4</sub><sup>2-</sup> ions in the precursor is less than that of C<sub>12</sub>H<sub>25</sub>SO<sub>4</sub><sup>-</sup> ions, which are preferential in attracting the surplus VO<sup>2+</sup> (Table 1A). First of all, owing to the characteristic of hydrophilicity and hydrophobicity, C<sub>12</sub>H<sub>25</sub>SO<sub>4</sub><sup>-</sup> ions form spherical micelles, with negative charge on the surface. At the same time, the dominant positive VO<sup>2+</sup> ions are attracted by the negatively charged C<sub>12</sub>H<sub>25</sub>SO<sub>4</sub><sup>-</sup> spherical micelles,<sup>44,45</sup> so the VO<sup>2+</sup> ions can cover them, forming crystal seeds. Then the rest neutral VOC<sub>2</sub>O<sub>4</sub> nucleates and grows into nanowires on the surface of the spherical micelles through heterogeneous nucleation. Meanwhile, the spherical micelles merge with each other and grow up under high temperature and pressure condition. With the increase of the reacting time, VO<sub>2</sub> nanowires grow longer and longer around the spherical micelles and the carbon layer *in situ* covers the surface of VO<sub>2</sub> nanowires homogeneously. At last, hollow microspheres can be obtained after washing mildly with deionized water and alcohol to remove the C<sub>12</sub>H<sub>25</sub>SO<sub>4</sub><sup>-</sup> spherical micelles. Thus, hollow microspheres are achieved through the charge balance of the negatively charged C<sub>12</sub>H<sub>25</sub>SO<sub>4</sub><sup>-</sup> spherical micelles and moderate VO<sup>2+</sup> positive ions.

Then time-dependent comparison experiments were also implemented to identify the formation process of VO<sub>2</sub> six-armed microspindles, when the molar ratio of V<sub>2</sub>O<sub>5</sub> and H<sub>2</sub>C<sub>2</sub>O<sub>4</sub> is 1:3.0. The reacting time increases from 6 to 12, 18, and 24 h, respectively (Figure 2B). It clearly shows that spindlelike particles are first obtained with a diameter of 500–800 nm and a length of ~2 μm when the reacting time is 6 h (Figure 1B1 and Figure S7A,B). More interestingly, a lot of grooves are found on the surface of the spindlelike particles and become clear and uniform with the increase of the reacting time (Figure 1B2,3 and Figure S7C,D). After reacting 24 h, the homogeneous six-armed microspindles are obtained, with three nanosheets intersecting with each other and the intersection angle is ~60° (Figure 1B4 and Figure S7E,F). The hollow spindlelike particles are also obtained when proper amount of hydrochloric acid is added (Figure S8A,B),<sup>46</sup> and the surface of cross section of six-armed microspindles is very smooth (Figure S8C,D). On the basis of above results, combined with the understanding of Ostwald-ripening process, the formation process can be illustrated as follows (Figure 1B). As shown in the eqs 1–3, V<sub>2</sub>O<sub>5</sub> and H<sub>2</sub>C<sub>2</sub>O<sub>4</sub> completely react with each other in the molar ratio of 1:3. The dominant positive ion is VO<sup>2+</sup>, which is also proved by the blue color of the precursor solution (Figure S6) and the dominant negative ion is C<sub>2</sub>O<sub>4</sub><sup>2-</sup> (Table 1B). First, C<sub>12</sub>H<sub>25</sub>SO<sub>4</sub>Na dissolves in the precursor solution to reduce the surface energy which is conducive to the crystallization. Then the VOC<sub>2</sub>O<sub>4</sub> nucleate and grow into spindlelike particles,<sup>33,46–48</sup> with grooves on the surface resulting from the erosion of the adequate oxalic acid. After that, the weak crystal orientations are corroded and dissolved; meanwhile, the strong crystal orientations recrystallize and regrow. According to Goodenough's description, the essential

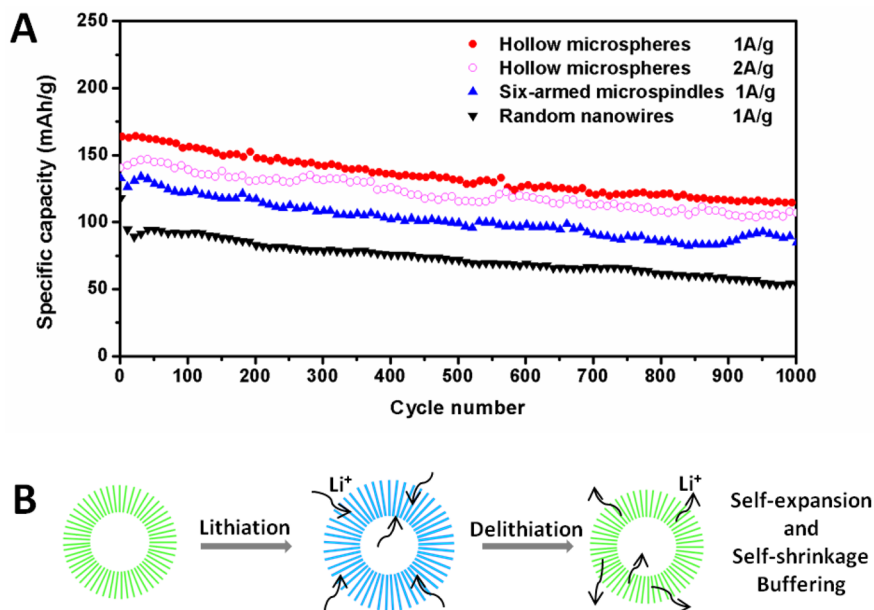


**Figure 3.** (A) Cycling performance of  $\text{VO}_2$  hollow microspheres, six-armed microspindles, and random nanowires, at current densities of 1 and 2 A/g in 2–3 V. (B) Schematic of  $\text{VO}_2$  hollow microspheres structure during lithiation and delithiation.

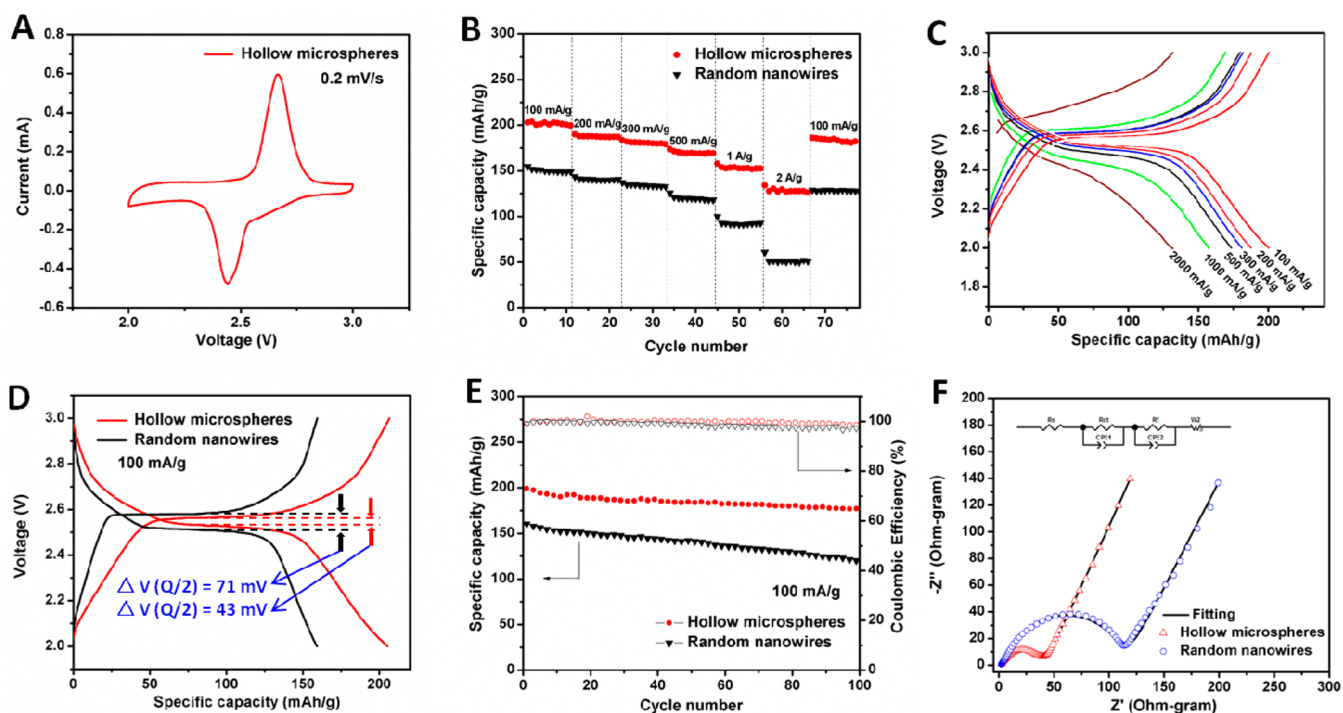


**Figure 4.** Electrochemical characterizations of  $\text{VO}_2$  hollow microspheres and random nanowires. (A) CV curve of hollow microspheres in 2–3 V at a scan rate of 0.2 mV/s. (B) Rate performance of hollow microspheres and random nanowires in 2–3 V. (C) Charge–discharge curves of hollow microspheres at different current densities. (D) The first charge–discharge curve of hollow microspheres and random nanowires at 100 mA/g. (E) Cycling performance of hollow microspheres and random nanowires at 100 mA/g in 2–3 V. (F) AC impedance plots of hollow microspheres and random nanowires after 10 cycles.

electronic structure of monoclinic  $\text{VO}_2$  has been retained as nanostars.<sup>49,50</sup> Finally, the spindle-like particles are transformed into six-armed microspindles, which should result from the synergistic effect of the acid erosion and outside-in oriented Ostwald-ripening process.<sup>39</sup>

When the molar ratio of  $\text{V}_2\text{O}_5$  and  $\text{H}_2\text{C}_2\text{O}_4$  increases to 1:1.8, only a small part of  $\text{V}_2\text{O}_5$  is reduced, which is also demonstrated by the light green color of the precursor (Figure

S6). The main positive ions are  $\text{VO}_2^+$  and  $\text{VO}^{2+}$  (Table 1C).  $\text{VO}^{2+}$  ions are attracted in priority by  $\text{C}_2\text{O}_4^{2-}$  ions, while  $\text{Na}^+$  ions are attracted in priority by  $\text{C}_{12}\text{H}_2\text{SO}_4^-$  ions owing to the Coulomb electrostatic law. So vanadium oxide ions grow into random nanowires owing to the oriented growth (Figure S9).

Then the electrochemical performance of these nanostructures is characterized.<sup>51</sup> At the current density of 1 A/g, the original capacity of hollow microspheres is 163 mAh/g, higher

than those of six-armed microspindles and random nanowires (142 and 118 mAh/g), respectively. After 1000 cycles, 73% of the original capacity of hollow microspheres is retained, while the capacity retentions of six-armed microspindles and random nanowires are only 60% and 45%, respectively (Figure 3A). Particularly, at high current density of 2 A/g, 80% of the original capacity of hollow microspheres is maintained after 1000 cycles, showing high-rate and long-life cycling performance. Even at low current density of 100 mA/g, 90% of the initial capacity of hollow microspheres is kept after 100 cycles (Figure 4E), while the capacity retention of random nanowires is only 75%. Because VO<sub>2</sub> hollow microspheres show empty spherical core with radially protruding nanowires, the nanowires separate from each other on one side and are interconnected with each other on the other side, which greatly increase the electrode–electrolyte contact area and shorten the pathways for lithium ion diffusion. The Brunauer–Emmerr–Teller (BET) surface area of hollow microspheres is 22.3 m<sup>2</sup>/g, about 2 times higher than 12.3 m<sup>2</sup>/g of random nanowires. Furthermore, in order to confirm their stability, the coin cells were taken apart after the electrochemical performance test. Only hollow microspheres structure keeps intact after the test (Figure S10), which provides a free volume for self-expansion and self-shrinkage during lithiation/delithiation (Figure 3B), efficiently inhibiting the self-aggregation of nanowires. However, a part of six-armed microspindles are pulverized and most of random nanowires self-aggregate after 1000 cycles at 1 A/g (Figures S9 and S10).

To understand why this novel architecture exhibits such excellent cycling performance, more electrochemical measurements are performed. Cyclic voltammetry (CV) measurement is performed to characterize the phase transformation and ionic diffusion process during electrode reactions in 2–3 V at a scan rate of 0.2 mV/s (Figure 4A). Hollow microspheres exhibit only one pair of well-defined anodic and cathodic peaks, corresponding to the galvanostatic cycling test (Figure 4D). The overpotential is measured from the difference between charge and discharge potential at the half reversible capacity, noted as  $\Delta V(Q/2)$ .<sup>37</sup> The overpotential of hollow microspheres is only 43 mV, which is much lower than 71 mV of random nanowires, showing higher electrical and ionic conductivity and deep insights are confirmed as follows. First, electrochemical impedance spectroscopy (EIS) measurement is carried out. The charge transfer resistance ( $R_{ct}$ ) of hollow microspheres is only 39  $\Omega$  after 10 cycles, while the corresponding  $R_{ct}$  of random nanowires is 111  $\Omega$  (Figure 4F), suggesting their fast electronic mobility. Second, the peak voltages in CV at different scan rates are tested. According to the Randles–Sevick equation,<sup>52</sup> the diffusion coefficient of hollow microspheres is about  $4.84 \times 10^{-7}$  cm<sup>2</sup>/s (Figure S11), while the previously reported VO<sub>2</sub> ribbons is  $10^{-9}$ – $10^{-10}$  cm<sup>2</sup>/s.<sup>31</sup> Third, the carbon layer coated on the surface can protect the structure from dissolution and enhance the conductivity effectively. Then the rate performances are compared (Figure 4B). A specific discharge capacity of 203 mAh/g of hollow microspheres is obtained at 100 mA/g; after testing at the current densities of 200, 300, 500, 1000, and 2000 mA/g, 93% of the original capacity is recovered when coming back to 100 mA/g, while the recovery ratio of random nanowires is only 76%. The capacity of hollow microspheres is 134 mAh/g at 2 A/g, about 3 times higher than that of random nanowires (46 mAh/g). The charge–discharge curves of hollow microspheres are consistent with the CV measurement (Figure 4C), showing

a stable platform at each current density, and hollow microspheres also keep higher discharge capacity and show more stable cycling performance than those of random nanowires at 300 and 500 mA/g (Figure S12). These results demonstrate that the hollow microspheres exhibit excellent structural stability and cyclability at low and high current densities, suggesting their fast kinetics for lithium ion intercalation–deintercalation.

In summary, hollow microspheres having empty spherical core with radially protruding VO<sub>2</sub> nanowires are constructed through a facile controllable ion-modulating approach. The formation processes have been illustrated and confirmed by controlling different dominant positive and negative ions in the precursor. Hollow microspheres assembled with VO<sub>2</sub> nanowires exhibit highest capacity and excellent cyclability due to their high surface and efficient self-expansion and self-shrinkage buffering. This structure can accommodate the volume variation and release the strain during lithium intercalation–deintercalation, effectively inhibiting the self-aggregation of nanowires. Our results demonstrate that hollow microspheres are highly promising in high-rate and long-life lithium batteries. Meanwhile, this facile and controllable ion-modulating method can be generally applied to fabricate other nanomaterials and nanostructures and has the great potential for large-scale applications.

## ■ ASSOCIATED CONTENT

### Supporting Information

Additional information and figures. This material is available free of charge via the Internet at <http://pubs.acs.org>.

## ■ AUTHOR INFORMATION

### Corresponding Authors

\*E-mail: mlq518@whut.edu.cn (L.M.).

\*E-mail: hch5927@whut.edu.cn (C.H.).

### Author Contributions

<sup>†</sup>These authors contributed equally to this work.

### Notes

The authors declare no competing financial interest.

## ■ ACKNOWLEDGMENTS

This work is supported by the National Basic Research Program of China (2013CB934103, 2012CB933003), the International Science and Technology Cooperation Program of China (2013DFA50840), the National Natural Science Foundation of China (51272197, 51302203), the Fundamental Research Funds for the Central Universities (2013-ZD-7), and the Students Innovation and Entrepreneurship Training Program (1366601001, 20131049701002). Thanks to Prof. C. M. Lieber of Harvard University and Prof. D. Y. Zhao of Fudan University for strong support and stimulating discussions.

## ■ REFERENCES

- (1) Yao, J.; Yan, H.; Lieber, C. M. *Nat. Nanotechnol.* **2013**, *8*, 329.
- (2) Tang, J. Y.; Huo, Z. Y.; Brittan, S.; Gao, H. W.; Yang, P. D. *Nat. Nanotechnol.* **2011**, *6*, 568.
- (3) Wu, H.; Chan, G.; Choi, J. W.; Ryu, I.; Yao, Y.; McDowell, M. T.; Lee, S. W.; Jackson, A.; Yang, Y.; Hu, L. B.; Cui, Y. *Nat. Nanotechnol.* **2012**, *7*, 310.
- (4) Duan, X. J.; Fu, T. M.; Liu, J.; Lieber, C. M. *Nano Today* **2013**, *8*, 351.
- (5) Mai, L. Q.; Xu, L.; Han, C. H.; Xu, X.; Luo, Y. Z.; Zhao, S. Y.; Zhao, Y. L. *Nano Lett.* **2010**, *10*, 4750.

- (6) Han, C. H.; Pi, Y. Q.; An, Q. Y.; Mai, L. Q.; Xie, J. L.; Xu, X.; Xu, L.; Zhao, Y. L.; Niu, C. J.; Khan, A. M.; He, X. Y. *Nano Lett.* **2012**, *12*, 4668.
- (7) Jiang, J.; Li, Y. Y.; Liu, J. P.; Huang, X. T.; Yuan, C. Z.; Lou, X. W. *Adv. Mater.* **2012**, *24*, 5166.
- (8) Li, W.; Deng, Y. H.; Wu, Z. X.; Qian, X. F.; Yang, J. P.; Wang, Y.; Gu, D.; Zhang, F.; Tu, B.; Zhao, D. Y. *J. Am. Chem. Soc.* **2011**, *133*, 15830.
- (9) Cao, A. M.; Hu, J. S.; Liang, H. P.; Wan, L. J. *Angew. Chem., Int. Ed.* **2005**, *44*, 4391.
- (10) Wu, C. Z.; Xie, Y.; Lei, L. Y.; Hu, S. Q.; Ouyang, C. Z. *Adv. Mater.* **2006**, *18*, 1727.
- (11) Wang, T. Y.; Peng, Z.; Wang, Y. H.; Tang, J.; Zheng, G. F. *Sci. Rep.* **2013**, *3*.
- (12) Hwang, Y. J.; Wu, C. H.; Hahn, C.; Jeong, H. E.; Yang, P. D. *Nano Lett.* **2012**, *12*, 1678.
- (13) Teng, Z. G.; Zheng, G. F.; Dou, Y. Q.; Li, W.; Mou, C. Y.; Zhang, X. H.; Asiri, A. M.; Zhao, D. Y. *Angew. Chem., Int. Ed.* **2012**, *124*, 2215.
- (14) Pan, A. Q.; Wu, H. B.; Yu, L.; Lou, X. W. *Angew. Chem., Int. Ed.* **2013**, *52*, 2226.
- (15) Liu, J.; Xie, C.; Dai, X. C.; Jin, L. H.; Zhou, W.; Lieber, C. M. *Proc. Natl. Acad. Sci. U. S. A.* **2013**, *110*, 6694.
- (16) Yang, C.; Zhao, H. B.; Hou, Y. L.; Ma, D. *J. Am. Chem. Soc.* **2012**, *134*, 15814.
- (17) Qie, L.; Chen, W. M.; Xu, H. H.; Xiong, X. Q.; Jiang, Y.; Zou, F.; Hu, X. L.; Xin, Y.; Zhang, Z. L.; Huang, Y. H. *Energy Environ. Sci.* **2013**, *6*, 2497.
- (18) Yang, J. P.; Shen, D. K.; Zhou, L.; Li, W.; Li, X. M.; Yao, C.; Wang, R.; El-Toni, A. M.; Zhang, F.; Zhao, D. Y. *Chem. Mater.* **2013**, *25*, 3030.
- (19) Xu, L.; Jiang, Z.; Qing, Q.; Mai, L. Q.; Zhang, Q. J.; Lieber, C. M. *Nano Lett.* **2013**, *13*, 746.
- (20) Ge, M. Y.; Lu, Y. H.; Ercius, P.; Rong, J. P.; Fang, X.; Mecklenburg, M.; Zhou, C. W. *Nano Lett.* **2014**, *14*, 261.
- (21) Liu, B.; Zeng, H. C. *J. Am. Chem. Soc.* **2004**, *126*, 8124.
- (22) Sun, Y. M.; Hu, X. L.; Luo, W.; Xia, F. F.; Huang, Y. H. *Adv. Funct. Mater.* **2013**, *23*, 2436.
- (23) Li, L.; Wang, H. Q.; Fang, X. S.; Zhai, T. Y.; Bando, Y.; Golberg, D. *Energy Environ. Sci.* **2011**, *4*, 2586.
- (24) Yang, S. H.; Lin, X.; Blake, A. J.; Walker, G. S.; Hubberstey, P.; Champness, N. R.; Schröder, M. *Nat. Chem.* **2009**, *1*, 487.
- (25) Soegiarto, A. C.; Comotti, A.; Ward, M. D. *J. Am. Chem. Soc.* **2010**, *132*, 14603.
- (26) Chhowalla, M.; Shin, H. S.; Eda, G.; Li, L. J.; Loh, K. P.; Zhang, H. *Nat. Chem.* **2013**, *5*, 263.
- (27) Whittingham, M. S. *Chem. Rev.* **2004**, *104*, 4271.
- (28) Chernova, N. A.; Roppolo, M.; Dillon, A. C.; Whittingham, M. S. *J. Mater. Chem.* **2009**, *19*, 2526.
- (29) Yao, H. B.; Zheng, G. Y.; Li, W. Y.; McDowell, M. T.; Seh, Z. W.; Liu, N.; Lu, Z. D.; Cui, Y. *Nano Lett.* **2013**, *13*, 3385.
- (30) Mahmood, N.; Zhang, C. Z.; Liu, F.; Zhu, J. H.; Hou, Y. L. *ACS Nano* **2013**, *7*, 10307.
- (31) Yang, S. B.; Gong, Y. J.; Liu, Z.; Zhan, L.; Hashim, D. P.; Ma, L. L.; Vajtai, R.; Ajayan, P. M. *Nano Lett.* **2013**, *13*, 1596.
- (32) (A) Popuri, S. R.; Miclau, M.; Artemenko, A.; Labrugere, C.; Villesuzanne, A.; Pollet, M. *Inorg. Chem.* **2013**, *52*, 4780. (B) Krakowiak, J.; Lundberg, D.; Persson, I. *Inorg. Chem.* **2012**, *51*, 9598.
- (33) Zhao, J. Z.; Tao, Z. L.; Liang, J.; Chen, J. *Cryst. Growth Des.* **2008**, *8*, 2799.
- (34) Liu, J. P.; Jiang, J.; Bosman, M.; Fan, H. J. *J. Mater. Chem.* **2012**, *22*, 2419.
- (35) Yan, M. Y.; Wang, F. C.; Han, C. H.; Ma, X. Y.; Xu, X.; An, Q. Y.; Xu, L.; Niu, C. J.; Zhao, Y. L.; Tian, X. C.; Hu, P.; Wu, H. A.; Mai, L. Q. *J. Am. Chem. Soc.* **2013**, *135*, 18176.
- (36) Mai, L. Q.; Yang, F.; Zhao, Y. L.; Xu, X.; Xu, L.; Luo, Y. Z. *Nat. Commun.* **2011**, *2*, 381.
- (37) Mai, L. Q.; Wei, Q. L.; An, Q. Y.; Tian, X. C.; Zhao, Y. L.; Xu, X.; Xu, L.; Chang, L.; Zhang, Q. *J. Adv. Mater.* **2013**, *25*, 2969.
- (38) Wang, Y. L.; Wang, T. Y.; Da, P. M.; Xu, M.; Wu, H.; Zheng, G. F. *Adv. Mater.* **2013**, *25*, 5177.
- (39) (A) Uchaker, E.; Gu, M.; Zhou, N.; Li, Y. W.; Wang, C. M.; Cao, G. Z. *Small* **2013**, *9*, 3880. (B) Pan, A. Q.; Liu, J.; Zhang, J. G.; Gao, G. Z.; Xu, W.; Nie, Z. M.; Jie, X.; Choi, D.; Arey, B. W.; Wang, C. M.; Liang, S. Q. *J. Mater. Chem.* **2011**, *21*, 1153.
- (40) Chen, J.; Cheng, F. Y. *Acc. Chem. Res.* **2009**, *42*, 713.
- (41) Synthesis methods of these three nanostructures are as follows: V<sub>2</sub>O<sub>5</sub> (2 mmol), various amounts of H<sub>2</sub>C<sub>2</sub>O<sub>4</sub>·2H<sub>2</sub>O and C<sub>12</sub>H<sub>25</sub>SO<sub>4</sub>Na (1.7 mmol) were added into 33 mL of H<sub>2</sub>O, stirred for 24 h at 40 °C until homogeneous liquid was obtained. Then it was transferred into a 50 mL Teflon autoclave and kept at 180 °C for different reaction times. After cooling to room temperature, the final products were successfully obtained by washing mildly with pure alcohol and deionized water several times and drying at 70 °C in air for 24 h. Characterizations: The crystallographic information of the final products was measured by a D8 Advance XRD using Cu K $\alpha$  radiation in a 2 $\theta$  range from 10° to 90° at room temperature. FESEM images were observed by a JEOL-7100F; TEM and HRTEM images were observed by a JEM-2100F. BET surface area was measured using a Tristar-3020 instrument by adsorption of nitrogen at 77 K. EDS was recorded by using an Oxford EDS IE250. TG-DSC was measured by a STA-449C.
- (42) Huo, Q. S.; Margolese, D. I.; Ciesla, U.; Feng, P. Y.; Gier, T. E.; Sieger, P.; Leon, R.; Petroff, P. M.; Schüth, F.; Stucky, G. D. *Nature* **1994**, *368*, 317.
- (43) Kresge, C. T.; Leonowicz, M. E.; Roth, W. J.; Vartuli, J. C.; Beck, J. S. *Nature* **1992**, *359*, 710.
- (44) Wu, Z. C.; Zhang, M.; Yu, K.; Zhang, S. D.; Xie, Y. *Chem.—Eur. J.* **2008**, *14*, 5346.
- (45) Zeng, H. C. *Curr. Nanosci.* **2007**, *3*, 177.
- (46) Kanie, K.; Muramatsu, A. *J. Am. Chem. Soc.* **2005**, *127*, 11578.
- (47) Jia, C. J.; Sun, L. D.; Yan, Z. G.; You, L. P.; Luo, F.; Han, X. D.; Pang, Y. C.; Zhang, Z.; Yan, C. H. *Angew. Chem., Int. Ed.* **2005**, *44*, 4328.
- (48) Bai, F.; Wang, D. S.; Huo, Z. Y.; Chen, W.; Liu, L. P.; Liang, X.; Chen, C.; Wang, X.; Peng, Q.; Li, Y. D. *Angew. Chem., Int. Ed.* **2007**, *46*, 6650.
- (49) Goodenough, J. B. *J. Solid State Chem.* **1972**, *5*, 1972.
- (50) Whittaker, L.; Velazquez, J. M.; Banerjee, S. *CrystEngComm* **2011**, *13*, 5328.
- (51) Electrochemical measurements: the electrochemical performance was characterized with 2016 coin cells assembled in a glovebox filled with pure argon gas. Lithium foil was used as the anode; a solution of LiPF<sub>6</sub> (1 M) in EC/DEC (1:1 vol/vol) was used as the electrolyte; 70% active materials, 20% acetylene black, and 10% poly(tetrafluoroethylene) (PTFE) were composed and grinded as cathode. Galvanostatic charge/discharge measurement was performed with a multichannel battery testing system (LAND CT2001A); CV and EIS were measured by an Autolab potentiostat galvanostat at room temperature.
- (52) Jung, H. G.; Hassoun, J.; Park, J. B.; Sun, Y. K.; Scrosati, B. *Nat. Chem.* **2012**, *4*, 579.